CHEMISTRY OF MATERIALS

ARTICLE

pubs.acs.org/cm

A New Form of $LiNbO_3$ with a Lamellar Structure Showing Reversible Lithium Intercalation

V. Pralong,*[,†] M. Anji Reddy,[†] V. Caignaert,[†] S. Malo,[†] O. I. Lebedev,[†] U. V. Varadaraju,[‡] and B. Raveau[†]

[†]Laboratoire CRISMAT, CNRS, 6 Bd Maréchal Juin, F-14050 Caen 4, France

[‡]Materials Science Research Centre, Indian Institute of Technology Madras, Chennai 6000 036, India

ABSTRACT: The exchange of lithium for univalent copper in $CuNbO_3$ has been investigated. A new form of $LiNbO_3$ with a lamellar structure has been synthesized from the topotactic reaction between $CuNbO_3$ and a molten salt corresponding to the eutectic "$LiCl/LiNO_3$". This compound crystallizes in the $P2_1/a$ space group with $a = 9.433$ Å, $b = 8.226$ Å, $c = 6.213$ Å, and $\beta = 90.2°$. This new phase intercalates one lithium on the first discharge and shows reversibility of 0.7 lithium through a first-order transformation leading to a capacity of 120 mAh/g at a potential of 1.65 V vs Li^+/Li.

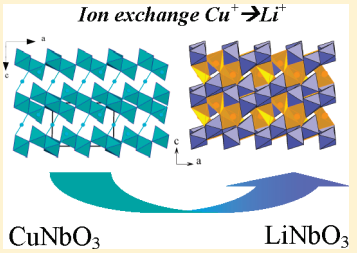

KEYWORDS: Li-ion batteries, $LiNbO_3$, lithium niobate, lithium insertion, exchange

INTRODUCTION

Among the numerous oxides that can be used as anode materials for rechargeable Li batteries, titanium- and niobium-based oxides continue to be considered as interesting candidates in spite of the low potential of the redox couple Ti^{4+}/Ti^{3+} and Nb^{5+}/Nb^{4+}, ranging from 1.2 V to 1.7 V. Indeed, these oxides are nontoxic and inexpensive and more importantly, their redox potential should avoid possible ignition of electrolyte in batteries.[1,2] On the basis of these considerations, the different forms of TiO_2 have been explored either as bulk materials[3] or as nanomaterials.[4−7] Similarly, spinel $Li_4Ti_5O_{12}$ was investigated and reported as a stable anode.[8,9] Mixed titanium−niobium oxides such as $Ti_2Nb_{10}O_{29}$,[10] $Ti_2Nb_2O_9$,[11] and $LiTiNbO_5$[12] were also shown to intercalate lithium with rather similar electrochemical performances.

In contrast, the number of studies of "pure" niobium oxides or niobates is more limited. Lithium insertion in Nb_2O_5 was demonstrated,[13] but the various forms of this oxide were more studied for their electrochromic properties. The facile lithium intercalation in the perovskite $La_{0.33}NbO_3$,[14] and more recently in nanocrystalline $AlNbO_4$[15] and in the oxides KNb_5O_{13} and $K_6Nb_{10.8}O_{30}$[16] with potential values ranging from 1.6 V for bulk to 1.2 V for nanocrystalline materials, suggests that niobates should be more deeply investigated.

We have thus considered the possibility to synthesize new structures in the Li−Nb−O system with an open framework susceptible to intercalate lithium reversibly, using soft chemistry methods. Here, we report a new form of $LiNbO_3$ with a lamellar structure that is synthesized from a topotactic reaction of $CuNbO_3$ with an eutectic $LiCl/LiNO_3$. We show that this niobate intercalates reversibly 0.7 lithium per formula unit (120 mAh/g) through a biphasic process at 1.6 V.

EXPERIMENTAL SECTION

Synthesis of $CuNbO_3$. $CuNbO_3$ was synthesized by a conventional solid-state reaction from the stoichiometric amounts of Cu_2O and Nb_2O_5. The initial reagents were first mixed and then heated at 950 °C for 12 h in a platinum crucible under argon flux. The X-ray powder diffraction pattern (Figure 1a) of the as prepared material $CuNbO_3$ corresponds to a well-crystallized phase already described by Marinder et al.[17] The samples we have synthesized always contain an impurity identified as $CuNb_3O_8$.[18]

Synthesis of $LiNbO_3$. Different attempts were made to synthesize topotactically $LiNbO_3$ from the oxide $CuNbO_3$, which was shown to exhibit a layered structure.[17] First, the possibility of exchange reaction in solution between LiCl or LiBr and $CuNbO_3$ using hexanol as solvent was considered. Whatever the experimental conditions, the exchange was unsuccessful. Thus, the possibility to exchange infused salt medium was tried. $CuNbO_3$ was mixed with an eutectic composition containing {39.3 wt % LiCl + 60.7 wt % $LiNO_3$}. The mixture was heated at 280 °C for 12 h. The resulting light green powder was washed with a HCl (2M) solution in order to eliminate the excess $LiCl/LiNO_3$ and the Cu_2O phase. It was filtered off and dried at 60 °C. For the above conditions, $LiNbO_3$ is obtained with a relatively good crystallinity as shown by the width of the reflections on the XRPD pattern (Figure 1b). Though the pattern of this phase seems at first sight rather different from that of $CuNbO_3$ (Figure 1a), it can be indexed to a rather similar cell, but with a different space group, as will be detailed further from the structure determination. EDS analysis performed with a SEM and atomic adsorption spectroscopy analysis allows us to confirm the cationic composition "LiNb", showing that all the copper had been exchanged, while the $CuNb_3O_8$ impurity remains unchanged in composition. The TGA-TDA analysis evidence an exothermal peak at 475 °C, without any weight loss up to 600 °C, showing a structural transition (not shown). The XRPD pattern of this phase, registered after this heat treatment, confirms that the layered $LiNbO_3$ form converts to the $LiNbO_3$ type structure[19] above 475 °C.

Structural Characterization. X-ray powder diffraction (XRPD) patterns were recorded in the 2θ range 5−120° using a Philips X'pert diffractometer with Bragg−Brentano geometry equipped with Cu Kα radiation. The pattern used for the structure refinement was registered with a Bruker D8 Advance diffractometer using Cu $K\alpha_1$ wavelength. For

Received: December 23, 2010
Revised: February 16, 2011
Published: March 09, 2011

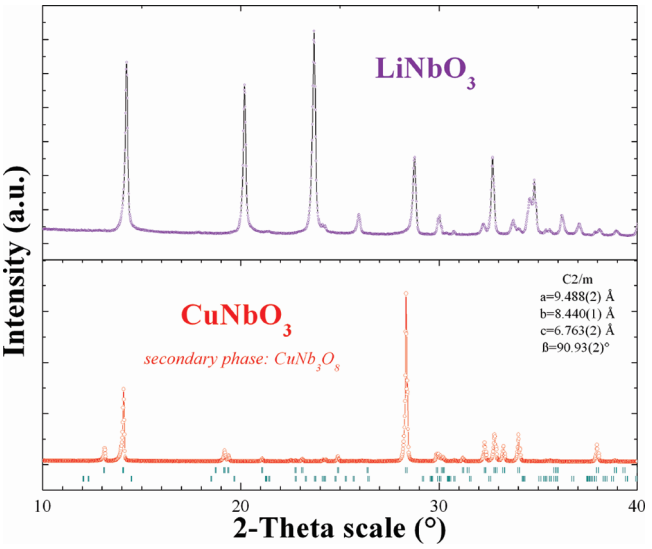

Figure 1. XRD pattern of $CuNbO_3$ and the phase obtained after ion exchange in LiCl−$LiNO_3$ eutectique at 280 °C.

the transmission electron microscopy study, the $LiNbO_3$ sample was crushed in alcohol, and the small flakes were deposited on a copper grid coated with holey carbon film. The electron diffraction (ED) studies were carried out on a JEOL 200CX electron microscope fitted with an eucentric goniometer (±60°) equipped with an EDS (energy dispersive spectroscopy) analyzer at room temperature, and a FEI TECNAI G^2 was used for HRTEM analysis. Image processing, and in particular Fourier transformation (FT), as well as computer image simulation was performed using the MacTempas software.

Chemical and Thermogravimetric analysis. The lithium content was determined by atomic absorption spectroscopy with a Varian Spectra AA-20 instrument. Thermogravimetric analysis (TGA) was performed in N_2 atmosphere at a heating rate of 5 °C/min with a TG92 Setaram microbalance.

Electrochemical Characterization. $LiNbO_3$ and carbon (carbon black 99.9%, Alfa Aesar) were taken in the weight ratio of 80:20 and ball milled for 2 h. Electrochemical studies were performed in Swagelok type cells. The cells were assembled in an argon filled glovebox. Lithium metal was used as the negative electrode, and a borosilicate glass fiber sheet (separator) was saturated with 1 M $LiPF_6$ in 1:1 ethylene carbonate (EC)/dimethyl carbonate (DMC) and used as electrolyte. Typically, each electrode contains 5−10 mg of the active material. The electrochemical studies were carried out at room temperature (RT) using a VMP II potentiostat/galvanostat (Biologic SA, Claix, France). Galvanostatic intermittent titration technique (GITT) measurements consisting of 2 h discharge at C/50 with open circuit periods of 1 h were performed. The potentiodynamic protocol used for the study was as follows. We performed a stepwise scanning of the potential, with 9 mV steps keeping the potential levels until the current has decayed to a preset minimum limit. Reaching this limit, that we express in terms of equivalent galvanostatic rate C/n, generates the next potential step. This stepwise potential protocol was first proposed by Thompson[20,21] in 1979 as electrochemical potential spectroscopy. It enables us to approach the thermodynamic characteristics of intercalation electrode materials if the limit current is chosen low enough (C/200 to C/500). Potentiostatic intermittent titration technique (PITT) measurements were conducted using potential steps of 9 mV limited by a minimum current equivalent to a C/20 galvanostatic rate. For ex situ XRD studies, approximately 100 mg of material was pressed into the shallow well of a SS plate. The Swagelok cells were assembled as described previously. The cells were discharged and charged to various stages at C/200. After the experiment the cells were dismantled in a glovebox, and the powder was collected. XRD patterns were recorded under vacuum by using a special chamber attached to the XRD instrument.

RESULTS AND DISCUSSION

Structure Determination. For the structure determination, the 20 first reflections of the XRPD pattern were indexed with the autoindexing software DICVOL6.[22] This program gave a unique monoclinic cell solution with high figures of merit, M(20) = 40[23] and F(20) = 39.[24] The cell parameters of this new form of $LiNbO_3$ are significantly different from those of $CuNbO_3$ (Table 1), as expected from the large difference in the patterns of these two compounds (Figure 1). Importantly, the electron diffraction study, carried out by tilting around the crystallographic axes, showed that this compound exhibits a different symmetry from that observed for $CuNbO_3$ ($C2/m$), i.e., corresponding to the $P2_1/a$ space group, as shown from the ED patterns registered along [100], [010] and [001] (Figure 2a). Indeed, no weak extra reflections corresponding to a doubling of the cell parameters (Table 1) were detected from this E.D. study, in contrast to the XRD single crystal results previously obtained for $CuNbO_3$.[17] The XRPD pattern of this phase, registered in reflection geometry, could be indexed to this space group and was then used to find the positions of niobium and oxygen atoms. The structure determination was revealed to be delicate for two reasons. First, very strong orientation phenomena were observed due to the layered character of the structure. The latter were considerably decreased by using the Debye−Scherrer configuration, i.e., with a thin layer of sample stuck with grease on the external surface of a Lindenman capillary. Second, as pointed out above, the XRPD pattern of the $LiNbO_3$ sample is very different from that of $CuNbO_3$. In particular, the number of intense reflections is much smaller than for $CuNbO_3$ (Figure 1). This is because the c parameter has considerably decreased with respect to $CuNbO_3$, making many reflections such as (110) and (001) practically superimposed in $LiNbO_3$, whereas they are clearly distinct in $CuNbO_3$. In addition, the monoclinic angle $\beta = 90.2°$ is so close to 90° that some reflections such as (111)/(−111) are practically superimposed in $LiNbO_3$. As a consequence, the refinement of the data of $LiNbO_3$ is made more difficult for $LiNbO_3$ than for $CuNbO_3$.

In spite of these difficulties, the Nb and O positions could be determined from ab initio structure calculation, using the FOX program,[26] and supposing that such a structure involves, like $CuNbO_3$, only NbO_6 octahedra. The structural model was built of two different Nb sites, and we used the dynamical occupancy feature, implemented in FOX, to take into account oxygen atoms shared between building blocks. A structure solution was found for $[NbO_3]_\infty$ layers of corner and edge-sharing octahedra, stacked along c, similarly to the parent structure $CuNbO_3$. The Rietveld refinement of the atomic positions of the NbO_3 framework using Fullprof[27] was more difficult for the lighter oxygen atoms. Thus, during the first cycles, constraints were applied to the O−O distances, which were imposed in a first step to be comprised between 2.40 and 2.90 Å in order to avoid divergence, then these constraints were released in a second step, refining simultaneously the Nb and O positions. Lithium positions cannot, of course, be obtained from XRD, but can be predicted by using the empirical bond valence rule.[28] Bond valence calculations were thus included in the FOX program and used as a cost function to optimize the valence of the elements as

Table 1. Crystallographic Data for $CuNbO_3$, $LiNbO_3$ 2D, and $LiNbO_3$ 3D

formula sum	$CuNbO_3$[17]	$LiNbO_3$ 2D [this work]	$LiNbO_3$ 3D[19]
formula weight	300.46 g/mol	147.846 g/mol	147.846 g/mol
crystal system	monoclinic	monoclinic	trigonal
space group	$C2/m$ (12)	$P2_1/a$ (14)	$R3c$ (161)
cell parameters	a = 9.488(2) Å, b = 8.440(1) Å, c = 6.763(2) Å, β = 90.93(2)°	a = 9.433(4) Å, b = 8.226(4) Å, c = 6.213(4) Å, β = 90.228(3)°	a = 5.1483(0) Å, c = 13.8631(4) Å
cell ratio	a/b = 1.1242 b/c = 1.2480 c/a = 0.7128	a/b = 1.1467 b/c = 1.3239 c/a = 0.6587	a/b = 1.0000 b/c = 0.3714 c/a = 2.6928
cell volume	541.50(21) Å^3	482.08(1) Å^3	318.21(1) Å^3
Z	8	8	6
calc. density	–	4.074 g/cm^3	–

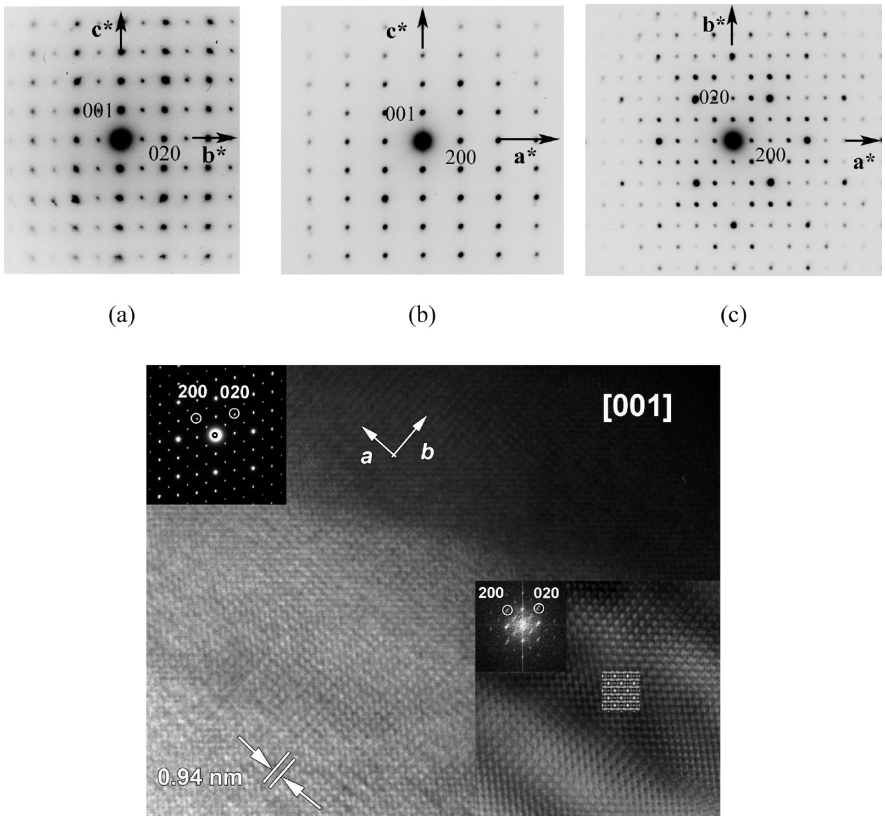

Figure 2. (a) ED patterns recorded along (a) [100], (b) [010], and (c) [001]. (d) [001] HRTEM image of $LiNbO_3$ structure and corresponding ED pattern. Bragg mask filtered image given as insert in the bottom, and simulated images based on the $P2_1/a$ (14) structure (See Table 1) are given as inset (Δf = −50 nm, t = 64 nm).

previously made for $Li_{12}Mo_5O_{17}$.[29] Two Li sites were then added at random in the unit cell, while positional parameters were kept fixed for the NbO_3 framework. A structure solution was found where Li^+ cations exhibit a valence close to +1 with two sorts of coordination, tetrahedral and pyramidal, respectively. It is worth mentioning that lithium has a too weak scattering factor to be refined by X-ray diffraction in such a complex structure, in the presence of much heavier atoms. It is then unrealistic to perform a Rietveld refinement of Li positions with our X-ray data. Nevertheless, we have added the two Li sites in the final refinement with a very strong damping coefficient on their atomic displacements. The Rietveld refinement of this model (Figure 3, Table 2) allowed a small but not significant improvement in the goodness of fit values: R_{wp} = 17.8%, R_B = 9.5%, and χ^2=2.76. The atomic coordinates (Table 3) can be considered as accurate for Nb and O, whereas Li positions are probable but remain hypothetical and will be the object of further investigations using neutron diffraction.

HRTEM measurements of this material are far from trivial because of its instability under the electron beam inside a microscope. Nevertheless, the [001] HRTEM image of this metastable phase (Figure 2b) shows bright dots that correspond to the channels, i.e., to the zones located at the border of the strips built up of ribbons of NbO_6 octahedra, whereas the much smaller and less bright spots correspond to the space between the octahedral ribbons. Attempts to simulate this image on the basis of the atomic positions previously determined from XRPD data lead to satisfactory results (insert in Figure 2b). The high instability of

dx.doi.org/10.1021/cm1036524 |*Chem. Mater.* 2011, 23, 1915–1922

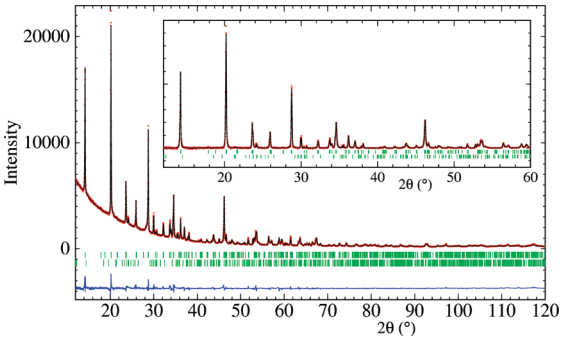

Figure 3. Rietveld refinement plot of $LiNbO_3$: observed X-ray diffraction intensity (○) and calculated curve (line). The bottom curve is the difference of patterns, $y_{obs} - y_{cal}$, and the small bars indicate the angular positions of the allowed Bragg reflections.

Table 2. Rietveld Refinement Results for 2D $LiNbO_3$

formula sum	$LiNbO_3$
formula weight	147.846 g/mol
crystal system	monoclinic
space group	$P2_1/a$ (14)
cell parameters	a = 9.433(4)Å, b = 8.226(4) Å,
	c = 6.213(4) Å, β = 90.228(3)°
cell ratio	a/b = 1.1467, b/c = 1.3239, c/a = 0.6587
cell volume	482.08(1) Å^3
Z	8
reflection number	357
refine parameters numbers	47
sample displacement	−0.0046
function profile	TCH
half width parameter	U = 0.039, V= −0.0003,
	W = 0.0000, Y = 0.0138
asymetrical parameters	0.0221/0.0210
R_{wp}, R_B, and χ^2	7.8%, 9.5%, 2.76

the material under e-beam inside the microscope results in a very noisy HRTEM image (Figure 2b). In order to increase signal/noise ratio, image processing using a Bragg reflection mask has been applied. The result is given as the insert in panel (b) of Figure 2 together with the corresponding FT pattern. The FT pattern (inset Figure 2b) confirms the ED report on panel (a) of Figure 2, which is consistent with the (001) zone. The presence of 010 and 100 diffraction spots on the FT pattern is characteristic of basically intact $LiNbO_3$ structure. In addition, the calculated image (see insert in Figure 2b) fits rather well the experimental one.

Structure Description. The structure of this new form of $LiNbO_3$ is directly derived from that of $CuNbO_3$. It consists of the stacking along c of very similar $[NbO_3]_\infty$ layers (Figure 4a). These (001) layers (Figure 4b), like those of $CuNbO_3$, consist of "Nb_4O_{16}" units of four edge-sharing NbO_6 octahedra. Each structural unit shares its eight corners with four other identical units, forming the $[NbO_3]_\infty$ layers. The Nb−O distances in the NbO_6 octahedra (Table 2) are rather similar in both structures, showing that the exchange of Li for Cu has not changed their geometry dramatically. The Nb1 octahedra located inside the Nb_4O_{16} structural unit exhibit Nb−O distances ranging from

Table 3. Atomic Coordinates of Niobium, Lithium, and Oxygen in $LiNbO_3$

atom	Wyck.	x/a	y/b	z/c	U [Å^2]
Nb1	4e	−0.0002(10)	0.1983(2)	−0.0073(10)	0.0070(7)
Nb2	4e	0.2418(3)	0.0038(10)	0.2584(4)	0.0138(9)
O1a	4e	0.375(2)	0.152(2)	0.086(3)	0.0086(18)
O1b	4e	0.3619(18)	0.840(3)	0.177(3)	0.0086(18)
O2a	4e	0.1113(17)	0.843(2)	0.295(3)	0.0086(18)
O2b	4e	0.097(2)	0.186(2)	0.245(3)	0.0086(18)
O3	4e	0.1313(15)	−0.008(3)	0.9468(19)	0.0086(18)
O4	4e	0.3255(18)	−0.031(3)	0.539(3)	0.0086(18)
Li1	4e	0.96754(7)	0.68040(6)	0.51081(14)	0.0237
Li2	4e	0.73023(7)	0.85565(7)	0.24030(12)	0.0237

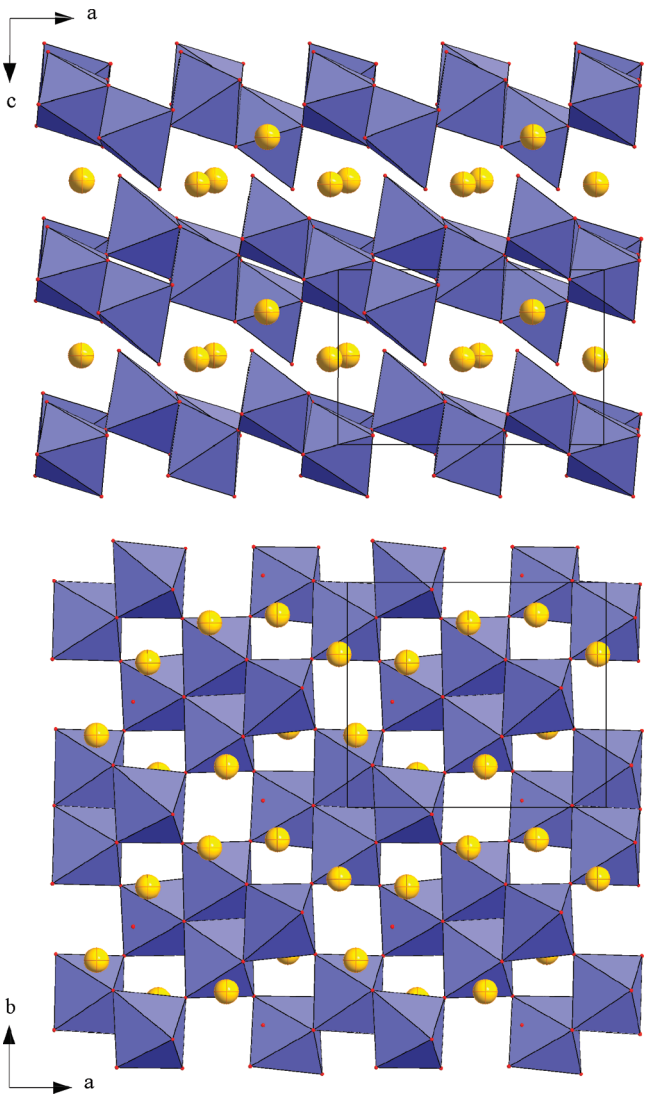

Figure 4. $LiNbO_3$. (a) View of the structure along b, showing the stacking of the (001) $[NbO_3]_\infty$ layer. (b) Perspective view of one $[NbO_3]_\infty$ layer along c. (c) Perspective view along c of the LiO_4 and LiO_5 polyhedra.

1.80 to 2.12 Å (compared to 1.83 to 2.13 Å for $CuNbO_3$), whereas for the Nb2 octahedra, which have one free apex, the

dx.doi.org/10.1021/cm1036524 |*Chem. Mater.* 2011, 23, 1915–1922

Table 4. Selected Distances for $LiNbO_3$

Nb1	O1a	1*x*	1.80	O2b	Nb1	1*x*	1.81
	O2b	1*x*	1.81		Li1	1*x*	1.97
	O3	1*x*	2.03		Nb2	1*x*	2.02
	O1b	1*x*	2.04		O3	1*x*	2.46
	O2a	1*x*	2.09	O3	Nb1	1*x*	2.03
	O3	1*x*	2.12		Nb1	1*x*	2.12
Nb2	O2a	1*x*	1.82		Li2	1*x*	2.15
	O1b	1*x*	1.83		Nb2	1*x*	2.19
	O4	1*x*	1.93		O2b	1*x*	2.46
	O2b	1*x*	2.02		O2a	1*x*	2.49
	O1a	1*x*	2.05	O4	Li1	1*x*	1.82
	O3	1*x*	2.19		Nb2	1*x*	1.93
O1a	Nb1	1*x*	1.80		Li2	1*x*	2.05
	Nb2	1*x*	2.05	Li1	O4	1*x*	1.82
	Li2	1*x*	2.25		O2b	1*x*	1.97
O1b	Nb2	1*x*	1.83		O1b	1*x*	2.30
	Nb1	1*x*	2.04		O2a	1*x*	2.33
	Li2	1*x*	2.07	Li2	O2a	1*x*	2.01
	Li1	1*x*	2.30		O4	1*x*	2.05
	O2a	1*x*	2.47		O1b	1*x*	2.07
O2a	Nb2	1*x*	1.82		O3	1*x*	2.15
	Li2	1*x*	2.01		O1a	1*x*	2.25
	Nb1	1*x*	2.09				
	Li1	1*x*	2.33				
	O1b	1*x*	2.47				
	O3	1*x*	2.49				
O2b	Nb1	1*x*	1.81				

niobium cation is slightly more off-centered with Nb−O distances ranging from 1.82 to 2.19 Å (against 1.78 to 2.27 Å for $CuNbO_3$). Thus, the main difference of the $LiNbO_3$ structure with respect to $CuNbO_3$ deals with the interlayer distances that are much shorter, i.e., 6.21 Å instead of 6.76 Å in $CuNbO_3$. This is easily explained by the different nature of the intercalated species, in contrast to Cu^+, which adopts a linear configuration; Li^+ accommodates generally a tetrahedral or an octahedral coordination, or eventually an intermediate 5-fold coordination. This viewpoint is corroborated by the BVS calculations, which suggest for lithium two kinds of coordination: a distorted tetrahedral coordination for Li1 with Li−O distances ranging from 1.82 to 2.33 Å, and a distorted pyramid for Li2 with Li−O distances ranging from 2.01 to 2.25 Å (Table 4). The lithium form with oxygen a layered "LiO_3" lattice of corner-sharing LiO_4 and LiO_5 polyhedra.

Electrochemical Properties of $LiNbO_3$. The electrochemical study of $LiNbO_3$ shows its ability to intercalate one Li per formula. The charge discharge profiles have been performed by a galvanostatic cycling at C/10 in the potential window 1.0−3.0 V versus Li/Li^+ (Figure 5). The first discharge involves the insertion of one lithium, leading to the formula Li_2NbO_3. After the first cycle, a reversible capacity of 0.7Li/f.u. (120 mAh/g) is obtained at an average potential of 1.65 V. As shown on the derivative curve (inset of Figure 5), the sharp redox peaks occurring around 1.65 V exhibit a low polarization of about 40 mV in cycling. The potentiodynamic titration curve (PITT, Figure 6) reveals a bell shape type response on the reversible phenomena, and confirms together with the sharpness of the peaks in the derivative curve that the reversible process is

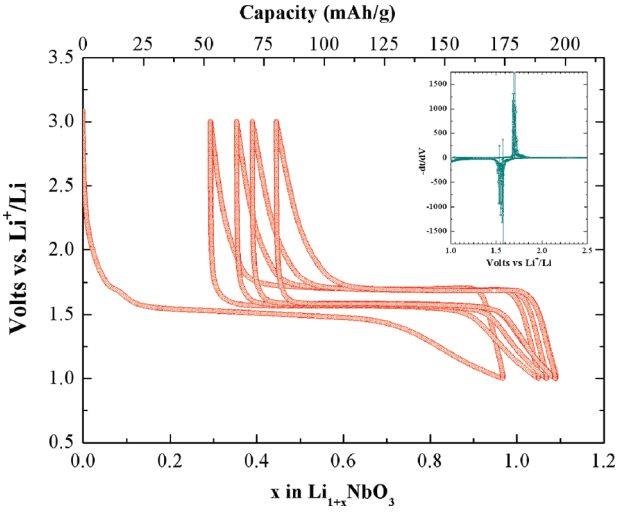

Figure 5. (a) $LiNbO_3$: Potential vs capacity curve at C/10 in the 3−1 V potential window. Inset: Corresponding incremental capacity d*t*/d*V* vs potential curve of the 2nd cycle.

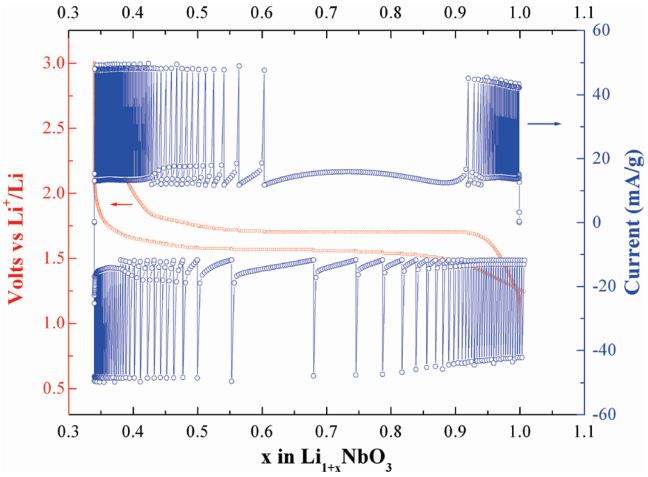

Figure 6. Potentiometric titration curve (PITT) during the second cycle of $LiNbO_3$ in the range of 3.0−1.0 V vs Li^+/Li limitation of the 9 mV potential step in duration of 1 h and current limitation equivalent to a galvanic current $I_{limit} = I_{C/20}$.

biphasic. Indeed, the evolution of the current reflects the displacement of the interface under the overpotential from the two-phase equilibrium potential (1.65 V), with a possible evolution of its area, which usually increases at the beginning and decreases as the phase transformation tends to be completed. For a given potential, the current is constant as a function of time during several steps, with a current value proportional to ΔV regarding to a transformation potential close to 1.65 V. This type of response is observed for both, in solid/solid and solid/solution transformations, and characterizes a first-order transformation limited by the progress of the interface area.[30,31] We performed also intermittent galvanostatic cycling (GITT) using a galvanostatic rate of C/20 for 2 h and then 2 h relaxation. The biphasic process is also confirmed by a GITT measurement (Figure 7) because a stable potential of 1.63 V on charge and 1.65 V on discharge is reached on relaxation. Finally, the plot of discharge capacity versus cycle number (Figure 8) indicates a drop of capacity after the first cycle, followed by a stable

dx.doi.org/10.1021/cm1036524 |*Chem. Mater.* 2011, 23, 1915–1922

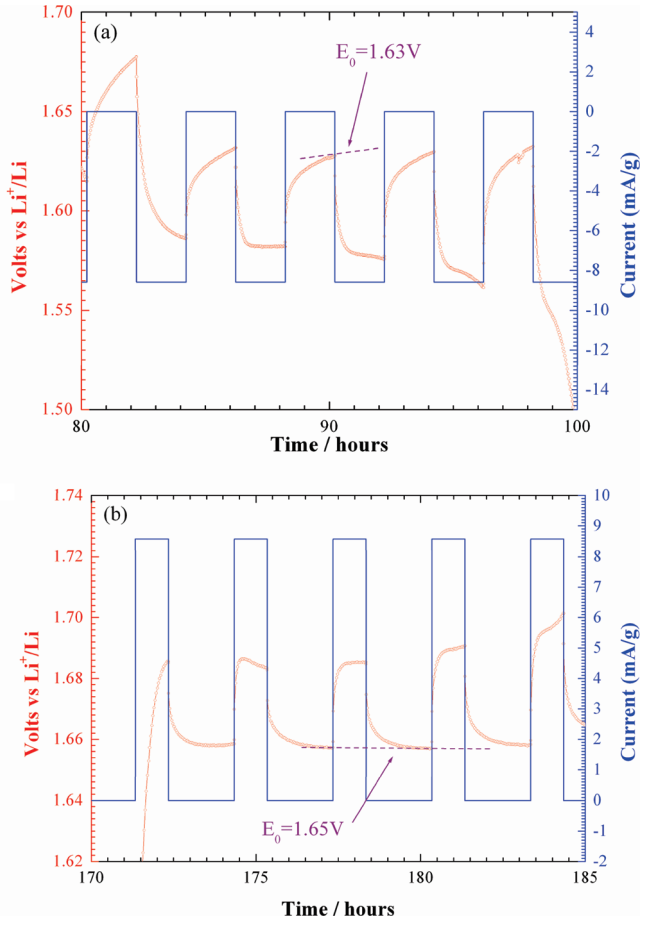

Figure 7. Intermitent galvanostatic titration (GITT) curve for the second (a) charge and (b) discharge.

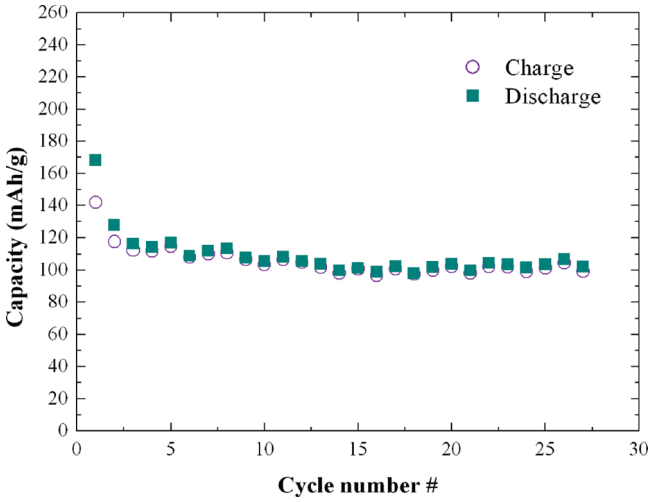

Figure 8. Specific discharge capacity vs cycle number of $LiNbO_3$. The potential window is 3−1.0 V, and the cycling rate is C/10.

reversible capacity of 110 mAh/g even after 20 cycles for a C/10 rate. Thus, we find that $LiNbO_3$ can reversibly intercalate 0.7 Li through a first-order transformation at 1.65 V.

The XRPD patterns of the discharged (1 V) and charged (3 V) phases are reported in Figure 9. The fully discharged phase with

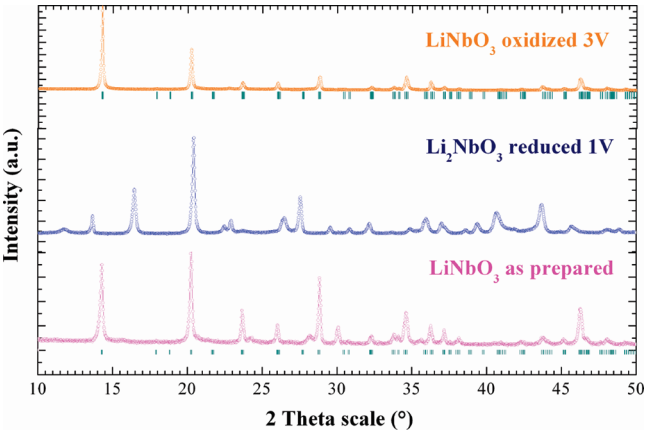

Figure 9. Powder X-ray diffraction patterns of (a) pristine $LiNbO_3$, (b) electrochemically discharged phase Li_2NbO_3, and (c) electrochemically charged phase $LiNbO_3$ 3.0 V (C/20).

the nominal composition of "Li_2NbO_3" shows a complete change in the reflections position suggesting a structural change. Then, a detailed neutron diffraction study will be required in order to understand the structural modification due to the lithium insertion. The complete reversibility of the electrochemical process is confirmed by the fact that the oxidized phase reveals the same position of the reflection as the mother phase. Note that the (00l) peaks present a different intensity, compared to the as prepared $LiNbO_3$ phase, due to a strong preferential orientation.

Electrochemical Properties of $CuNbO_3$. The electrochemical intercalation of lithium into $CuNbO_3$ was performed at C/10 rate, discharging the cell down to 1.0 V. The corresponding galvanostatic discharge curve (Figure 10a) shows that 1.8 lithium ions can be inserted per formula, but only one lithium is reversibly deintercalated. Importantly, one observes two phenomena: the first discharge associated with a broad peak on the derivative curve and subsequent cycling, associated then to sharp peaks on the derivative curve (Figure 10b). In order to have a better insight into the transformation occurring in the course of the first discharge, a chemical reduction was performed in argon filled glove using 200 mg of $CuNbO_3$ in 10 mL solution of 2.5 M *n*-buthyl lithium (*n*Bu-Li) in hexane stirring at room temperature for 3 days (equiv −2.0 V vs ENH). Note therefore the *n*Bu-Li was used as reducing agent of niobium oxides in previous studies.[11,12] The resulting XRD pattern is reported in panel (c) of Figure 10. One can observe that the lithium insertion is in fact accompanied by the formation of metallic copper according to the following equation

$$CuNbO_3 + (1+x)Li^+ + (1+x)e^- \rightarrow Li_{(1+x)}NbO_3 + Cu^0 \quad (x \sim 0.50)$$

From the electrochemical curve, it seems that such a phenomenon is not reversible. It is also worth noting that a complete reduction would lead to the phase Li_2NbO_3. However, the reduced phase is poorly crystallized and shows a strong anisotropic peak shape due to the lamellar character of the parent phase and also to the lithium insertion that generates strains. In these conditions, it is quite difficult to refine properly the XRD pattern of the fully reduced phase. Interestingly, such a behavior is not without reminding the extraordinary reversible Li-driven Cu

dx.doi.org/10.1021/cm1036524 |*Chem. Mater.* 2011, 23, 1915–1922

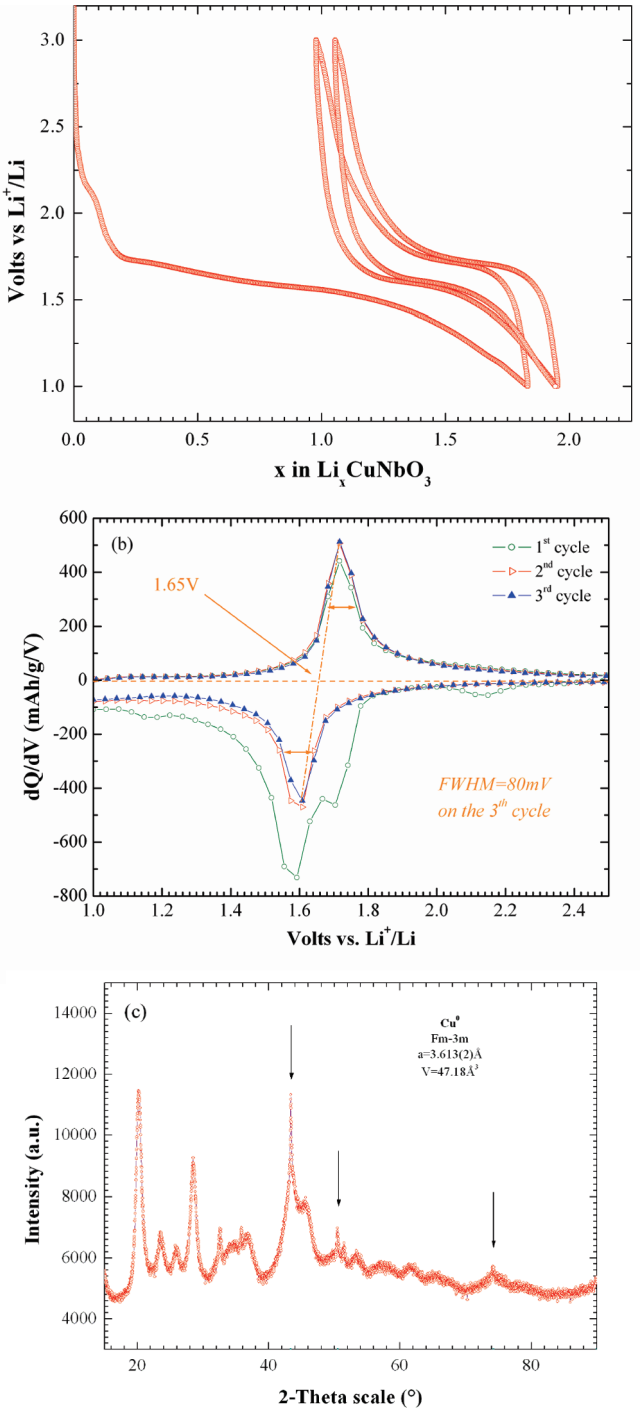

Figure 10. (a) $CuNbO_3$: Potential vs capacity curve at C/10 in the 3−1 V potential window. (b) Corresponding incremental capacity d*x*/d*V* vs potential curve of the 2nd cycle. (c) XRD pattern of the fully reduced "$Li_{1.5}CuNbO_3$" obtained from chemical reduction of $CuNbO_3$. Note the presence of Cu^0 reflections.

extrusion/injection of Cu in $Cu_{2.33}V_4O_{11}$ discovered by Morcrette et al.,[32] in which the fully discharged material was a mixture of lithiated vanadium oxide and metallic copper. Interestingly, the same group shows that such phenomena are occurring in lamellar niobium oxides such as $CuNb_2O_6$ or $Ag_2Nb_4O_{11}$[33], but in these cases without any reversibility of the copper injection in the course of further charge.

CONCLUSION

This study shows the promising possibility to exchange lithium for univalent copper in oxides, using soft chemistry methods. In this way, a new polymorph of $LiNbO_3$ with a 2D structure has been synthesized for the first time. The electrochemical behavior of this new phase is quite attractive, showing its ability to intercalate up to 1 Li per formula at 1.65 V, with a good reversible capacity of ∼110 mAh/g over 20 cycles. Other monovalent cation ion exchanges such as Na^+ will be explored further.

AUTHOR INFORMATION

Corresponding Author

*E-mail:valerie.pralong@ensicaen.fr. Tel: +33 2 31 45 26. Fax: +33 2 31 95 16 00.

ACKNOWLEDGMENT

The authors thank Dr. N. Barrier for the XRD registration of the capillary and Prof. G. Van Tendeloo for study available through the microscopy platform. Financial support from IFCPAR (Indo-French Centre for the Promotion of Advanced Research/Centre Franco-Indien Pour la Promotion de la Recherche Avancee) is gratefully acknowledged.

REFERENCES

(1) Whittingham, M. S. *Chem. Rev.* **2004**, *104* (10), 4271–4302.
(2) Bruce, P. G. *Solid State Sci.* **2005**, *7*, 1456.
(3) Armstrong, A. R.; Armstrong, G.; Canales, J.; Garcia, R.; Bruce, P. G. *Adv. Mater.* **2005**, *17*, 862.
(4) Hu, Y.-S.; Kienle, L.; Guo, Y.-G. *J. Adv. Mater.* **2006**, *18*, 1421.
(5) Reddy, M. A.; Kishore, M. S.; Pralong, V.; Varadaraju, U. V.; Raveau, B. *Electrochem. Solid State Lett.* **2007**, *10*, A29.
(6) Reddy, M. A.; Kishore, M. S.; Pralong, V.; Caignaert, V.; Varadaraju, U. V.; Raveau, B. *Chem. Matter.* **2008**, *20* (6), 2192–2197.
(7) Armstrong, G.; Armstrong, A. R.; Canales, J.; Bruce, P. G. *Electrochem. Solid State Lett.* **2006**, *9*, A139.
(8) Ferg, E.; Gummow, R. J.; De Kock, A.; Thackeray, M. M. *J. Electrochem. Soc.* **1994**, *141*, L147.
(9) Ohzuku, T.; Ueda, A.; Yamamoto, N. *J. Electrochem. Soc.* **1995**, *142*, 1431.
(10) Cava, R. J.; Murphy, D. W.; Zahurak, S. M. *J. Electrochem. Soc.* **1983**, *130* (12), 2345.
(11) Colin, J.-F.; Pralong, V.; Caignaert, V.; Hervieu, M.; Raveau, B. *Inorg. Chem.* **2006**, *45* (18), 7217–7223.
(12) Colin, J.; Pralong, V.; Hervieu, M.; Caignaert, V.; Raveau, B. *Chem. Mater.* **2008**, *20* (4), 1534–1540.
(13) Schmitt, M.; Heusing, S.; Aegerter, M. A.; Pawlicka, A.; Avellaneda, C. *Sol. Energy Mater. Sol. Cells* **1998**, *54*, 9.
(14) Wang, G. X.; Yao, P.; Bradhurst, D. H.; Dou, S. X.; Liu, H. K. *Solid State Ionics* **1999**, *124*, 37–43.
(15) Reddy, M. A.; Varadaraju, U. V. *Chem. Mater.* **2008**, *20*, 4557.
(16) Han, J.-T.; Liu, D.-Q.; Song, S.-H.; Kim, Y.; Goodenough, J. B. *Chem. Mater.* **2009**, *21*, 4753–4755.
(17) Marinder, B.-O.; Wahlstrom, E. *Chem. Scr.* **1984**, *23*, 157.
(18) Marinder, B. O.; Werner, P. E.; Wahlstrom, E.; Malmros, G. *Acta Chem. Scand., Ser. A* **1980**, *34*, 51.
(19) Abrahams, S. C.; Reddy, J. M.; Bernstein, J. L. *J. Phys. Chem. Solids* **1966**, *27*, 997–1012.
(20) Thompson, A. H. *J. Electrochem. Soc.* **1979**, *126*, 603.
(21) Thompson, A. H. *Rev. Sci. Instrum.* **1983**, *54*, 329.
(22) Boultif, A.; Louer, D. *J. Appl. Cryst,.* **2004**, *37*, 724.
(23) De Wolff, P. M. *J. Appl. Crystallogr.* **1968**, *5*, 108.
(24) Smith, G. S.; Snyder, R. L. *J. Appl. Crystallogr.* **1979**, *12*, 60.
(25) Favre-Nicolin, V.; Cerny, R. *J. Appl. Crystallogr.* **2002**, *35*, 734.

(26) Cerny, R.; Favre-Nicolin, V. *Powder Diffraction* **2005**, *20*, 359.
(27) Rodriguez-Carvajal, J. *Phys. B.* **1993**, *192*, 55.
(28) Pannetier, J.; Bassas-Alsina, J.; Rodriguez-Carvajal, J.; Caignaert, V. *Nature* **1990**, *346*, 343.
(29) Pop, N.; Pralong, V.; Caignaert, V.; Colin, J. F.; Malo, S.; Van Tendeloo, G.; Raveau, B. *Chem. Matter* **2009**, *21*, 3242–3250.
(30) Southampton Electrochemistry Group. *Instrumental Methods in Electrochemistry*; Ellis Horwood Series in Physical Chemistry; Horwood Publishing, Ltd.: Chichester, U.K., 1985.
(31) Chabre, Y *Physics of Intercalation II*; NATO Science Series B; Springer: New York, **1993**; Vol. *305*, p 181.
(32) Morcrette, M.; Rozier, P.; Dupont, L.; Mugnier, E.; Sannier, L.; Galy, J.; Tarascon, J.-M. *Nat. Mater.* **2003**, *2*, 755–761.
(33) Rozier, P.; Morcrette, M.; Szajwaj, O.; Bodenez, V.; Dolle, M.; Surcin, C.; Dupont, L.; Tarascon, J. M. *Isr. J. Chem.* **2008**, *48*, 235.